UNIVERSITÄT AUGSBURG
Universitätsbibliothek

OPEN ACCESS
OPUS AUGSBURG

Excitability regulation in the dorsomedial prefrontal cortex during sustained instructed fear responses: a TMS-EEG study

Gabriel Gonzalez-Escamilla, Venkata C. Chirumamilla, Benjamin Meyer, Tamara Bonertz, Sarah von Grotthus, Johannes Vogt, Albrecht Stroh, Johann-Philipp Horstmann, Oliver Tüscher, Raffael Kalisch, Muthuraman Muthuraman, Sergiu Groppa

Angaben zur Veröffentlichung / Publication details:

Gonzalez-Escamilla, Gabriel, Venkata C. Chirumamilla, Benjamin Meyer, Tamara Bonertz, Sarah von Grotthus, Johannes Vogt, Albrecht Stroh, et al. 2018. "Excitability regulation in the dorsomedial prefrontal cortex during sustained instructed fear responses: a TMS-EEG study." *Scientific Reports* 8 (1): 14506. https://doi.org/10.1038/s41598-018-32781-9.

Nutzungsbedingungen / Terms of use:

CC BY 4.0

Dieses Dokument wird unter folgenden Bedingungen zur Verfügung gestellt: / This document is made available under these conditions:
CC-BY 4.0: Creative Commons: Namensnennung
Weitere Informationen finden Sie unter: / For more information see:
https://creativecommons.org/licenses/by/4.0/deed.de

SCIENTIFIC REPORTS

OPEN

Excitability regulation in the dorsomedial prefrontal cortex during sustained instructed fear responses: a TMS-EEG study

Received: 5 April 2018
Accepted: 11 September 2018
Published online: 28 September 2018

Gabriel Gonzalez-Escamilla[1], Venkata C. Chirumamilla[1], Benjamin Meyer[2], Tamara Bonertz[1], Sarah von Grotthus[1], Johannes Vogt[3], Albrecht Stroh[4], Johann-Philipp Horstmann[5], Oliver Tüscher[5], Raffael Kalisch[2], Muthuraman Muthuraman[1] & Sergiu Groppa[1]

Threat detection is essential for protecting individuals from adverse situations, in which a network of amygdala, limbic regions and dorsomedial prefrontal cortex (dmPFC) regions are involved in fear processing. Excitability regulation in the dmPFC might be crucial for fear processing, while abnormal patterns could lead to mental illness. Notwithstanding, non-invasive paradigms to measure excitability regulation during fear processing in humans are missing. To address this challenge we adapted an approach for excitability characterization, combining electroencephalography (EEG) and transcranial magnetic stimulation (TMS) over the dmPFC during an instructed fear paradigm, to dynamically dissect its role in fear processing. Event-related (ERP) and TMS-evoked potentials (TEP) were analyzed to trace dmPFC excitability. We further linked the excitability regulation patterns to individual MRI-derived gray matter structural integrity of the fear network. Increased cortical excitability was demonstrated to threat (T) processing in comparison to no-threat (NT), reflected by increased amplitude of evoked potentials. Furthermore, TMS at dmPFC enhanced the evoked responses during T processing, while the structural integrity of the dmPFC and amygdala predicted the excitability regulation patterns to fear processing. The dmPFC takes a special role during fear processing by dynamically regulating excitability. The applied paradigm can be used to non-invasively track response abnormalities to threat stimuli in healthy subjects or patients with mental disorders.

The dorsomedial prefrontal cortex (dmPFC) is involved in working memory, attention, emotion regulation and further distinct mental functions. Its role in threat processing has been repeatedly postulated[1,2]. Sustained fear situations are bounded to a well-defined stressor that will occur with some predictability in a short time window[3]. In instructed fear paradigms, a state of fear can be elicited by a cue when there is a contingency between it and a potentially dangerous stimulus. Previous functional (f)MRI studies have shown that evaluation of fearful stimuli lead to an activation of the dmPFC[2]. If excitatory or inhibitory mechanisms are involved or how a regulation of cortical excitability in the dmPFC during fear processing occurs is still unknown. These phenomena, however, play a crucial role for adaptive behavior in threat situations and their dysfunction could lead to the development of neuropsychiatric disorders.

[1]Section of Movement Disorders and Neurostimulation, Department of Neurology, Focus Program Translational Neurosciences (FTN), University Medical Center of the Johannes Gutenberg University Mainz, 55131, Mainz, Germany. [2]Neuroimaging Center Mainz, Focus Program Translational Neuroscience, University Medical Center of the Johannes Gutenberg University Mainz, 55131, Mainz, Germany. [3]Institute for Microscopic Anatomy and Neurobiology, University Medical Center of the Johannes Gutenberg University Mainz, 55131, Mainz, Germany. [4]Focus Program Translational Neurosciences, Institute for Microscopic Anatomy and Neurobiology, Johannes Gutenberg University Mainz, 55131, Mainz, Germany. [5]Department of Psychiatry and Psychotherapy, University Medical Center of the Johannes Gutenberg University Mainz, 55131, Mainz, Germany. Correspondence and requests for materials should be addressed to S.G. (email: segroppa@uni-mainz.de)

Event-related potential (ERP) analysis is an effective method to address neural processing and cortical excitability. The time-locked synchronous neural activity can be depicted as well during fear processing. One of the characterized ERP components to threat exposures is the P100, which reflects the non-conscious processing of presented cues. Conscious processing is linked to sustained attention and increasing use of processing resources[4] and involves the medial prefrontal cortex[5]. Fear responsiveness can be indexed by presence of the P300 and the longer-lasting late positive potential (LPP) components. LPP has been as well uniquely linked to memory encoding and storage during fear processing[6]. The LPP amplitude increases to threat stimuli; functional imaging studies showed activation of further nodes of the "fear network" (i.e. amygdala) interrelated to LPP magnitude. Electrophysiological LPP measures are therefore considered a viable marker of fear processing[7,8] and likely reflect summated neuronal activity of different regions conforming the fear network, given its sensitivity to a variety of task instructions and its long duration which appears not to habituate over repeated presentations of stimuli[9]. Specific causal manipulation through optogenetics in animal studies or transcranial magnetic stimulation (TMS) in humans could facilitate delimitation of the specific role of network nodes. Of note, the increased positivity of the LPP starting ~300–500 ms after stimuli presentation extends well beyond 1000 ms[10] and its duration is stimulus-guided, reflecting a continued physiological process related to attentional fear processing[11,12]. However, despite the importance of LPP to fear processing, its neural substrate is still not clear.

Here, we address dmPFC excitability by analyzing the LPP component through simultaneous TMS and EEG recordings during fear processing. Therefore, we adapted an instructed fear paradigm, where a conditioned stimulus (CS), called the CS+, predicts an unconditional fearful stimulus (US), while the other (the CS-) its absence. This paradigm has been previously applied to map the neural networks engaged in instructed fear showing an involvement of amygdala, insular cortex, the dmPFC, and the anterior cingulate cortex (ACC)[2,13,14]. During instructed fear the amygdala and the dmPFC are considered regulatory nodes for network responses to threat[2,15,16]. The dmPFC has been suggested to convey excitability regulation states during sustained fear events, via synchronized activity with other brain structures of the fear network[17]. Recent technical advances allow the non-invasive assessment of synchronized brain activity by TMS-EEG recordings at the brain surface level[18–21] and provide the opportunity to track physiological aspects of fear processing at the cortical level while also measuring long-range synchronization and excitability properties within the involved network nodes. In order to dissect and improve the EEG-based moderate spatial resolution for the characterization of the involved network, we link TMS-EEG responses to structural properties of the studied network as derived from MRI. Thereby, a precise temporal and spatial characterization of the dmPFC-guided fear processing is achieved.

Although the mechanisms underlying TEPs are not completely understood, they provide key information with respect to brain functions and networks involved in specific high-level cognitive processes. Indeed, recent efforts have been conducted to shed light on the mechanisms of TMS beyond the motor cortex[22–25] (see[26] for a recent review) and more specifically in the mPFC during different task[24,27]. Such studies have demonstrated TEPs to be highly reproducible to specific methodological contains[28,29] and to also be sensitive to changes in brain state. Therefore providing a quantifiable marker of the neurophysiological state of the cortex and important information regarding functional dynamics of distributed cortical networks[26]. Furthermore, the development of improved methods to obtain a reliable EEG source estimation should also provide spatial information on the evoked neural activity.

Results

Psycho-physiological markers of instructed fear responses. The behavioral ratings, obtained from the questionnaires of our instructed fear paradigm (Fig. 1), showed that the T condition lead to higher levels of expectancy for threat ($p < 0.001$, d' = 2.6) than NT cues. The captured heart rates were also markedly increased in T compared to the NT condition ($p < 0.001$, d' = 1.98) as shown in Fig. 2.

Cortical excitability-to-threat evoked potentials and dmPFC excitability modulation. Concordant with the results on the behavioral ratings and the heart rate frequency increase, the evoked peak amplitudes after the T visual cues were higher than for the NT trials in both the TMS and no-TMS experiments (Fig. 3). More specifically, after the visual cues we could identify two amplitude peaks that showed modulation. The first ERP component occurred at 152 ms (ERP152), followed by the LPP with an increased and sustained activity with high amplitude at 500 ms. In the no-TMS experiment, the LPP showed a sustained response beyond 1 s, decaying at ~1300 ms, whereas in the artefact-free filtered TMS–EEG data (1–30 Hz; TMS experiment) apart from the same two initial ERPs, additional and differential modulation of the EEG activity after the TMS pulse was observed. Here, six TMS-evoked potentials have been identified, TEP1 at 41 ms, TEP2 at 57 ms, TEP3 at 81 ms, TEP4 at 117 ms, TEP5 at 197 ms and TEP6 at 317 ms. The topographical distribution of the excitability-to-threat and the corresponding peak amplitudes for both T and NT conditions in the TMS experiment are shown in Fig. 3a,b.

When evaluating the evoked activity (Fig. 3, Table 1), the amplitude of the ERP152 did not differ between the T and NT conditions; whereas the LPP showed a significant increase in amplitude in the T condition ($p = 0.038$, Cohen's d = 0.5). After the TMS pulse, three of the TEPs showed amplitude differences between the two conditions: TEP41 ($p = 0.048$, d' = 0.47), TEP117 ($p = 0.049$, d' = 0.47), TEP197 ($p = 0.036$, d' = 0.51). The cluster analyses showed that the peaks of activity were accompanied by significant increases in the T condition when compared to the NT condition in the sensors corresponding to the frontal, dmPFC and central regions of different evoked potentials (Fig. 3b). The sustained positive activity after the LPP has been linked to the level of attention to relevant stimulus. The 25th and 75th percentiles of the signal-to-noise ratio (SNR) for the individual EEG signals were: −20 and 31 dB, with a median value of 11 dB. In this case, any of the obtained individual SNR values could be considered an outlier.

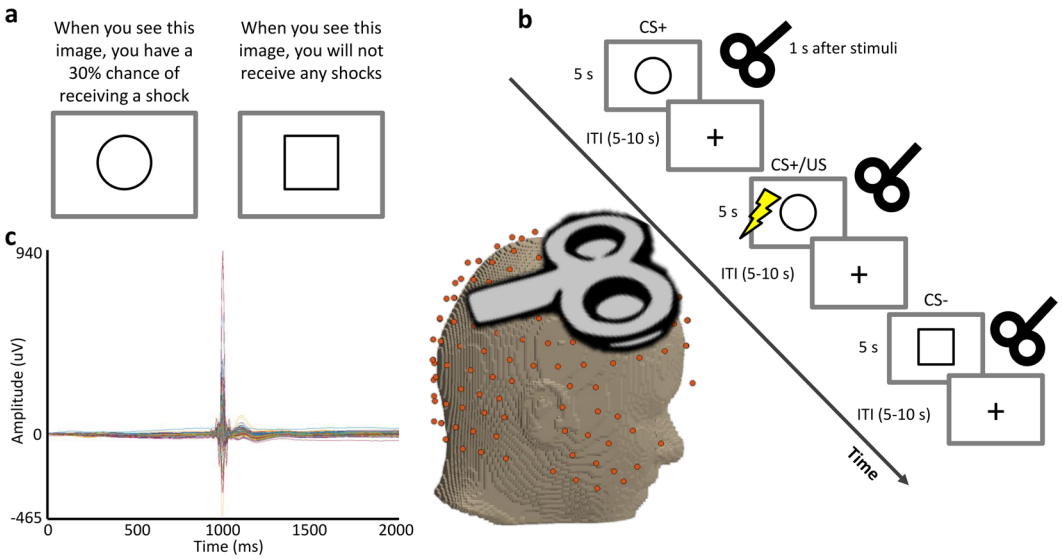

Figure 1. Experimental design. (**a**) Prior to the experimental phase, participants were informed about paradigm contingencies. (**b**) Schematic of the fear conditioning task. Three continuous blocks of trials were performed. In each block, one figure (the conditioned stimulus, or CS+) was paired with a shock (the unconditioned stimulus, or US) 33% of the time, whereas a second figure (the CS−) was never paired with a shock. Images were presented for 5 s, followed by a 5–10-second inter-stimulus interval (ITI). The figure represents the pseudorandom trial orders used during the experiment with the TMS stimuli applied 1 s after cue presentation in the case of the TMS experiments. (**c**) Butterfly plot showing an example of the EEG data with the TMS pulse visible.

Henceforth, we used the cortical excitability-to-threat, measured as the difference between threat and no-threat, and the dmPFC-related modulation in the subsequent analyses (Fig. 3c). In the case of the peak-to-peak amplitude latencies (Fig. 4), the LPP showed increased peak-to-peak amplitudes in respect to the ERP152 ($p = 0.014$, d' = 0.73). After the TMS stimulation, four peak-to-peak latencies showed significant changes: increased TEP41 compared to the TMS onset ($p = 0.022$, d' = 0.49), decreased TEP57 compared to TEP41 ($p = 0.042$; d' = 0.41), increased TEP81 compared to TEP57 ($p = 0.0025$, d' = 0.72) and increased TEP117 compared to TEP81 ($p = 0.015$, d' = 0.58).

When comparing the markers of cortical excitability in the two experiments, no significant changes were detected for the cortical excitability to T. Of note, increased excitability was evident after the TMS stimulation over the dmPFC (see topographies in Fig. 4). Moreover, the differences between conditions and peak-to-peak latencies showed a different temporal differentiation at different regions (Fig. 5). This result suggests a spread of activation from the dmPFC (stimulation site) to other interconnected areas, which are seen as deflections in the EEG signals.

Structural substrates of the excitability-to-threat and dmPFC-related modulation. The fear ratings were predicted by both right hippocampus and amygdala volumes ($r^2 = 0.3$, F = 3.65; $p = 0.048$). Furthermore, the volume of the left dmPFC and the right hippocampus correlated with the increase in heart rates in response to fear ($r^2 = 0.47$; F = 7.11; $p = 0.006$). As shown in Table 2, when examining associations between structural properties of the network nodes and the dmPFC excitability response to T, the integrity of the right dmPFC and the right amygdala predicted these measures. When analyzing the excitability-to-threat at the regional level, the structural integrity of the right dmPFC predicted the amplitudes of the evoked potentials after TMS. A similar effect was shown as well for several other structures in the network (i.e. insula; see also Supplementary Table 1 for more detailed information).

Discussion

In this work, we characterize excitability regulation patterns during an instructed fear paradigm non-invasively in healthy subjects. Threat processing is related to increased event-related activity with topological maximum in the dmPFC area. Furthermore, TMS pulses over the dmPFC induced a consistent modulation of the event-related activity with longer and increased threat-related responses. The threat-dependent excitability modulation was linked to the LPP component of evoked response. We found highly significant associations between evoked responses and markers of gray matter integrity, mainly in the dmPFC, but also in the amygdala and insula. The applied integrative approach illustratively describes the involved network. Our findings add to the current literature showing a pivotal role of the dmPFC in controlling the adaptive fear responses and introduce a non-invasive paradigm to measure physiological responses to threat[2]. Furthermore, the strong interrelation of excitability fingerprints, microstructural integrity and physiological markers of fear processing such as heart rate underpins

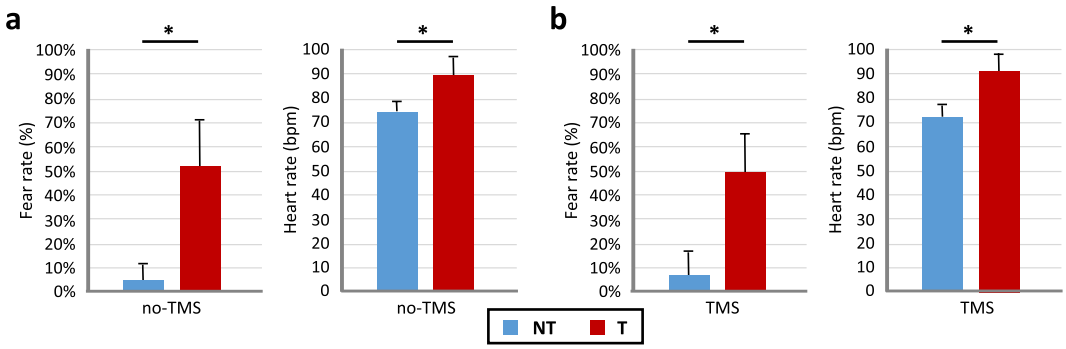

Figure 2. Hear rates and subjective fear ratings of the (**a**) no-TMS and (**b**) TMS experiments. The red bar represents T and blue bar represents NT conditions. The asterisk (*) denotes significant differences after correcting for multiple comparisons (FDR, $p < 0.05$).

the pivotal integrative value of the dmPFC in evaluative processes related to threat and the robust value of the introduced paradigm for causal interrogation of this specific node for fear processing.

The applied EEG approach permits an exact temporal characterization of threat processing. We see no delimitation of fear processing at early phases as quantified by ERP responsiveness at 152 ms (ERP152). And indeed at this very early stage merely the processing of complex visual information occurs and not the difference in the valence of the stimuli[30]. In our study, in both the TMS and no-TMS experiments increased threat-related excitability, as reflected by the appearance (and increase) of the LPP component, was detected. LPP is characterized by a sustained activity from ~500 ms and beyond ~1000 ms. Stimuli, most directly relevant to biological or imperative contents (threat, mutilation, etc), lead to an increase of LPP[31,32]. Emotional modulation of the LPP persists even after the full duration of stimulus presentation (e.g., 300–1500 ms) and shows several topographic shifts from parietal to central and frontal representations[4,33,34]. Moreover, LPP does not seem to habituate to emotional stimuli. Amygdala and prefrontal cortex activation have been described and related to attentional processing of emotional stimuli[35]. However, LPP amplitudes have been clearly shown to be linked to memory encoding and storage[30,36–39]. Similar to existing data showing poor correlation of the magnitude of early components (ERP152) with threat encoding, we only see consistent differences in the T-NT processing in the late components indexing distinct temporal facets of threat processing[9,36]. According to these findings, the LPP likely represents the summated activity of the entire network, thus through specific causal manipulation, which is possible using optogenetics in animal studies or TMS in humans, a specific role for each node of the fear network can be delimitated.

In our study, the LPP-evoked responses are further modulated by TMS pulses over the dmPFC, noticeable by the significantly higher amplitudes during the T condition with respect to the NT (also to the TMS experiment without task stimuli) and the evidenced fluctuation in the peak-to-peak amplitudes along the duration of the sustained response that was not present in the no-TMS experiment. This area might mediate the explicit evaluation of fear states and grant a controlled processing[16,40]. In concordance, larger LPP responses and increased dmPFC activations have been associated with amplified states of fear[2,41]. LPP increase and prolongation might mirror increased processing of the threat stimuli, while the dmPFC interferes with these processes.

TMS pulses induce well-described evoked potentials[42,43]; however, despite the groundwork that has been recently conducted[22–25] (see also[26] for a current review), more research is still needed to better understand the modulatory effects of TMS on the ongoing activity over cortical areas other than the motor cortex[26]. TEPs reflect the excitability of the cortex at the stimulated area and represent a summation of excitatory and inhibitory phenomena[44]. A recent work addressing TEP over prefrontal areas showed mainly an inhibitory effect of single-pulse TMS over the prefrontal cortex[42]. However, the evoked activity is more a complex interplay with possible interactions with excitatory neurotransmission for the early TEP peaks (10–30 ms) and inhibitory phenomena at later peaks (100–200 ms) as known for motor cortex stimulation[26]. Moreover, every TEP component presents a different topology suggesting a dynamic interaction of distinct cortical and subcortical areas.

In our study, the peak latency from ERP152-to-LPP is predicted by the volume of the right amygdala. Furthermore, the behavioral fear rates were predicted by the integrity of the right amygdala. Both findings support the role of the amygdala for fear evaluation and processing. These results are in good agreement with pivotal studies, showing that the activity of the amygdala was positively correlated with reports of anxiety[45]. The amygdala innervates the autonomic system, and thus is involved in the modulation of physiological responses to threat, aversive stimuli and signs of anxiety arousal, such as changes in heart rate[2,46]. Furthermore, the structural integrity of the paths connecting the amygdala to frontal regions predicts anxiety levels[15]. Similar to our study, recent work showed that threat events enhance dmPFC-amygdala connectivity[47], while the dmPFC possibly modulates amygdala activation, probably guided by inhibitory projections[48,49]. Here, these mechanisms were evidenced by both structural MRI and ERP analyses, highlighting not only a critical role of the dmPFC in regulating threat-related excitability, but also in recruiting interconnected regions of the fear network.

TMS pulses induce a spread of activation from the stimulation site to other interconnected brain areas, which are observed as deflections of the EEG signals (see for example Fig. 5). It is known that such effects start a few milliseconds after the pulse onset and last approximately 300 ms[50]. It has been suggested that the first TMS-evoked EEG activity reflects excitability, i.e. the functional state, of the stimulated area, whereas the following depicts the

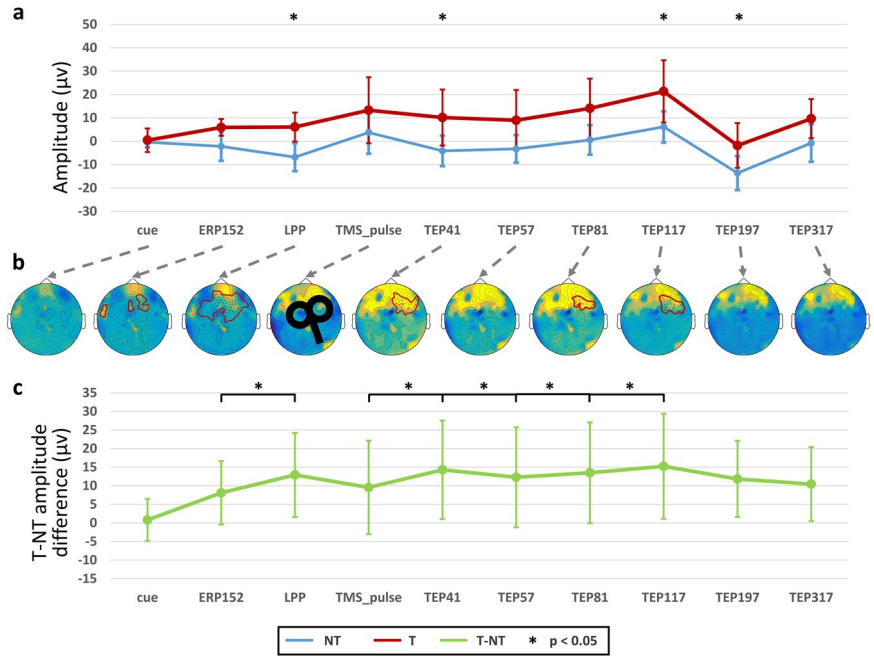

Figure 3. Event-related potentials (ERP) and TMS-evoked potentials (TEP). (**a**) Cortical excitability-to-threat (a.k.a. ERP) and dmPFC-related modulation peak (a.k.a. TEP) amplitude differences between the threat (T) and no-threat (NT) conditions over scalp electrodes. (**b**) Topographical distribution of the amplitude differences across the scalp, the red lines show the significant electrodes after cluster analysis (Monte Carlo permutations, $p < 0.05$). (**c**) Peak-to-peak amplitude latency differences for the cortical excitability-to-threat and dmPFC related modulation in the main experiment. In (**a**) and (**c**) the asterisk (*) denotes $p < 0.05$ after correcting for multiple comparisons.

	t	p	Mean Difference	SE Difference	Cohen's d
Psycho-physiological markers of instructed fear responses					
Heart rates	8.632	**<0.001**	2.395	0.277	**1.98**
Fear ratings	11.73	**<0.001**	0.465	0.04	**2.623**
Indicators of cortical excitability-to-threat and dmPFC modulation					
Cue (0 ms)	0.269	0.395	0.78	2.898	0.06
ERP152	1.86	**0.039**	8.096	4.353	**0.416**
LPP	2.235	**0.019**	12.891	5.769	**0.5**
TMS pulse	1.485	0.077	9.532	6.42	0.332
TEP41	2.113	**0.024**	14.273	6.756	**0.472**
TEP57	1.786	**0.045**	12.262	6.866	**0.399**
TEP81	1.951	**0.033**	13.496	6.918	**0.436**
TEP117	2.105	**0.024**	15.205	7.222	**0.471**
TEP197	2.258	**0.018**	11.814	5.232	**0.505**
TEP317	3.308	**0.002**	22.098	6.68	**0.74**
Peak-to-peak latencies					
0-to-ERP152	1.153	0.132	7.316	6.343	0.258
ERP152-to-LPP	2.375	**0.014**	4.795	2.019	**0.531**
LPP-to-TMS	0.726	0.762	3.359	4.627	0.162
TMS-to-TEP41	2.159	**0.022**	4.741	2.196	**0.483**
TEP41-to-TEP57	1.829	0.958	2.011	1.099	0.409
TEP57-to-TEP81	3.174	**0.002**	1.234	0.389	**0.71**
TEP81-to-TEP117	2.361	**0.015**	1.708	0.724	**0.528**
TEP117-to-TEP197	0.967	0.827	3.391	3.505	0.216
TEP197-to-TEP317	0.866	0.801	1.387	1.602	0.194

Table 1. Differences between Threat and no-Threat conditions in the TMS experiment. Contrast tested: Threat >no-Threat, bold text indicates significance after correction for multiple comparisons (FDR, $p < 0.05$).

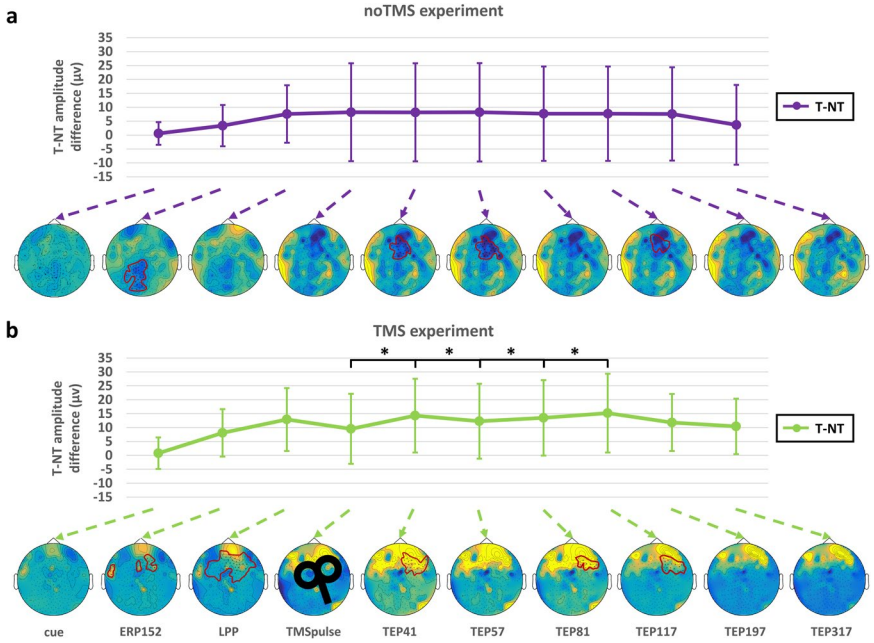

Figure 4. Comparison of cortical excitability-to-threat and the dmPFC-related modulation between TMS and no-TMS experiments. T-NT differences and their topographical representations in the (**a**) no-TMS (purple) and (**b**) TMS (green) experiments. The black lines indicate significant peak-to-peak latency changes in the TMS experiment with respect to the no-TMS experiment. At the bottom of each graph, the topographical distribution of the amplitude differences across the scalp is shown, where the red lines indicate the significant electrodes after cluster analysis (Monte Carlo permutations, $p < 0.05$). The asterisk (*) denotes significant differences after FDR correction ($p < 0.05$).

spread of activation to other cortical areas, likely reflecting the directedness or "effective" connectivity rising from the stimulated area[51,52]. Thus, the spatiotemporal deflections capture the modulation of the activity of functionally interacting neural assemblies. To verify such an assumption we therefore investigated the association of the evoked activity with the structural integrity of the regions part of the fear network. From these analyses mainly two regions showed up, namely the amygdala and dmPFC, strengthening their key role for fear processing and the existence of top-down modulatory mechanisms. All together, these findings highlight the promising ability of TMS-EEG to capture dynamical changes of cortico-cortical connectivity, identifying the segregation or the integration of particular brain areas during fear processing, which can be further extended to the study of other cognitive domains.

A limitation of the current study is the number of trials (36 per condition) for assessing TMS-evoked activity. However, recent evidence has shown that reliable measures of TMS excitability modulation can be obtained with even lower numbers of trials. More specifically, approximately 20–25 trials are suggested when neuronavigated stimulation is used for the study of cortical-excitability as induced by TMS-pulses over the motor cortex[28]; this has also been reported in recent meta-analyses[53]. Although these studies have used a lower number of trials to effectively study cortical excitability, given the analytical differences between motor-evoked responses and EEG-recorded activity, further studies are granted to shed light on this topic. In the current study, the SNR analysis showed low inter-individual variability in the evoked responses and as a result, the registered evoked activity can be considered of good quality. Ultimately, our findings provide the basis for possible mechanisms of fear processing which should be further explored in future studies.

Contrary to Pavlovian conditioning, in the applied fear paradigm the subjects are instructed about T and NT conditions before the experiment begins. Hence, for fear conditioning, learning takes place prior to stimuli exposure and fear processing requires controlled evaluation of fearful stimuli[54], likely with involvement of different areas of the fear network. Previous studies on instructed fear have consistently shown activations of the dmPFC, amygdala and ACC[2], however, robust measures of fear-related and dmPFC-modulated activation that are easy to apply in the clinical setting are still lacking. The dmPFC is not directly involved in the initial generation of fear responses but specifically modulate controlled/attended threat processing. Indeed, it has been shown that a loss of function in the dorsal mPFC regions is related to prolonged amygdala activation in persons with emotional dysregulation[14]. Moreover, prefrontal cortex excitability abnormalities have also been linked to impaired threat processing, anxiety and depression[55–57]. Taken together, these findings suggest that measures of dmPFC responses could evolve into a translational fingerprint that could be applied in experimental or clinical settings to dissect physiological from pathological responses or to monitor the transitional dynamics which provide resilience to mental illness. Furthermore, our results highlight the link between anatomical integrity and brain excitability patterns.

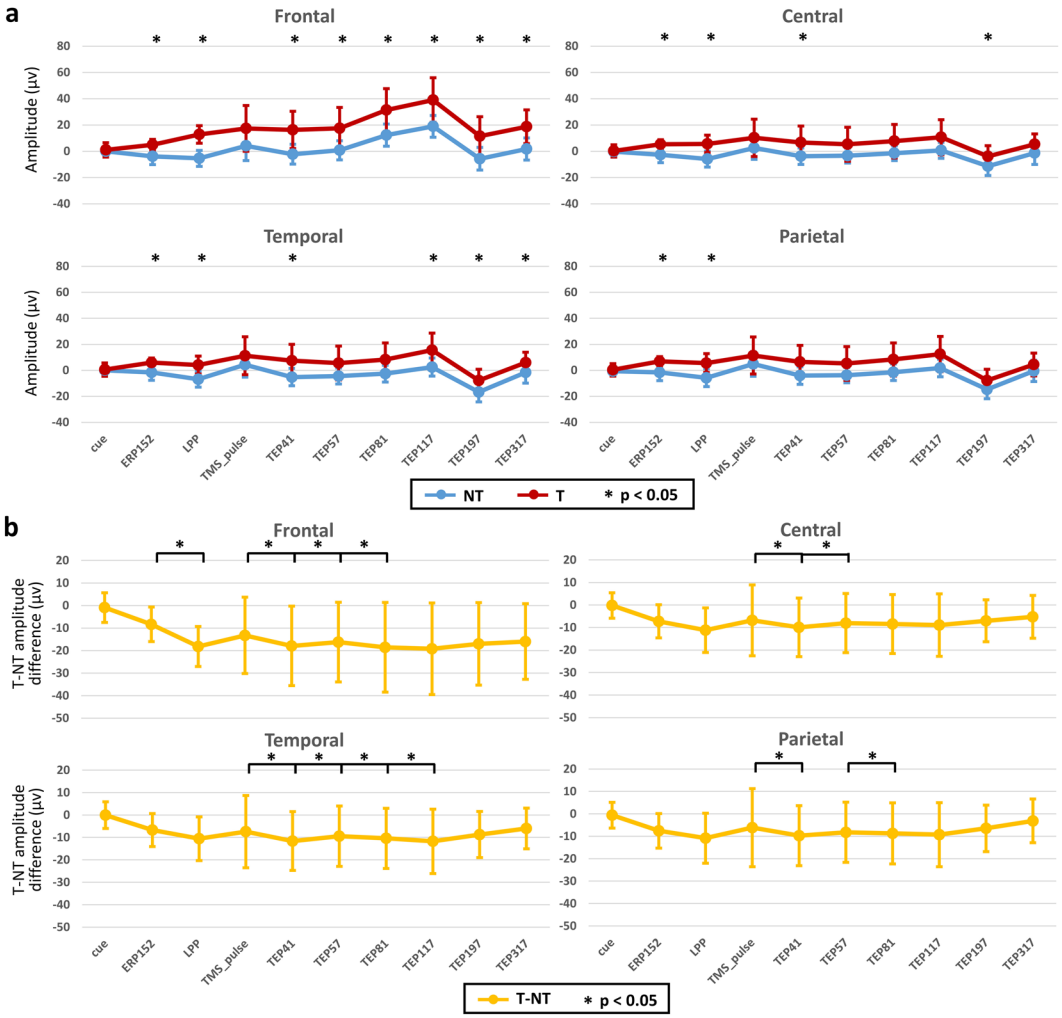

Figure 5. Regional event- and TMS-evoked potentials. (**a**) Amplitude peaks of the no-threat (NT) and threat (T) conditions. (**b**) Peak-to-peak latency activity of the excitability-to-threat and dmPFC-related modulation at different regions. The asterisk (*) denotes significant associations after correction for multiple comparisons (FDR, $p < 0.05$).

Conclusions

According to previous studies showing increased activation of the dmPFC during fear processing, the current paradigm allowed us to examine the specific role of dmPFC excitability regulation in healthy young subjects. TMS pulses over the right dmPFC during the instructed fear paradigm induced evoked responses with distinct temporal patterns linked to structural node properties of the fear network. This provides conclusive evidence for the involvement of the dmPFC in modulating the excitability-to-threat related to the long-lasting LPP component, a marker of fear stimuli processing, and sheds light on the role of the structural integrity in predicting different TMS-evoked activity peaks. Our results show causal evidence that fear processing requires higher cognitive mechanisms guided by the excitability properties of the dmPFC. Furthermore, our paradigm can be applied to test specific effects of dmPFC excitability modulation related to resilience and health.

Methods

Participants. In total, forty healthy young subjects were enrolled in the study. Twenty subjects participated in the designed main experiment (11 female; mean age ± SD: 26.8 ± 4.7 years). A second group of twenty healthy young subjects was used for a control experiment (11 female, mean age ± SD = 28.3 ± 6.6 years). The study was approved by the scientific and ethical committees at the University Medical Center Mainz and conducted in accordance with the ethical guidelines of the Declaration of Helsinki; all participants provided informed consent.

MRI data acquisition. Prior to the instructed fear paradigm, each participant underwent a standardized MRI scan. All MRI scans were acquired in a Siemens Trio 3 Tesla scanner (Siemens Medical Solutions, Erlangen, Germany). The T1 structural protocol was a magnetization-prepared rapid gradient-echo (MPRAGE) with the following parameters: repetition time [TR] = 1900 ms; echo time [TE] = 2.54 ms; inversion time [IT] = 900 ms; pixel bandwidth = 180; acquisition matrix = 320 × 320; flip angle = 9°; pixel spacing = 0.8125 × 0.8125 mm; slice thickness = 0.8 mm.

variable	Predicted by	r^2	adjusted r^2	F	*p*-value
Heart rates	lh dmPFC/rh Hp	0.47	**0.405**	7.114	**0.006**
Fear rates	rh Amy/rh Hp	0.3	**0.218**	3.653	**0.048**
Global analyses					
TEP41	rh dmPFC/rh Amy/lh Hp/rh Hp/lh Ins	0.72	**0.615**	7.066	**0.002**
TEP57	rh dmPFC/rh Amy/lh Hp/rh Hp/lh Ins	0.71	**0.604**	6.789	**0.002**
TEP81	rh dmPFC/rh Amy/lh Hp/lh Ins	0.63	**0.534**	6.443	**0.003**
TEP117	rh dmPFC/rh Amy/lh Hp/rh Hp/lh Ins	0.73	**0.639**	7.739	**0.001**
TEP197	rh dmPFC/rh Amy/lh Hp/lh Ins	0.65	**0.56**	7.054	**0.002**
TEP317	rh dmPFC/rh Amy/lh Ins	0.53	**0.439**	5.956	**0.006**
ERP152-to-LPP	rh Amy	0.23	**0.189**	5.436	**0.032**
LPP-to-TMS	lh Ins/rh Ins	0.3	0.212	3.561	0.051
TEP57-to-TEP81	rh dmPFC/lh Hp/rh Hp	0.51	**0.418**	5.551	**0.008**
TEP81-to-TEP117	rh dmPFC/rh Amy/rh Ins	0.43	**0.318**	3.957	**0.028**

Table 2. Step-wise regression analyses. lh = left hemisphere; rh = right hemisphere; Hp = hippocampus; Ins = insula; Amg = Amygdala; dmPFC = dorsomedial prefrontal cortex. Bold numbers indicate significant associations after correcting for multiple comparisons (FDR, $p < 0.05$).

Instructed fear paradigm. Before starting the experiment, the experimenter explicitly instructed all participants about the fear paradigm. During the sessions, an adapted version of the Raczka, *et al.*[58] instructed fear paradigm was applied, as previously described[59]. In the threat condition (T), a circle (conditioned stimulus, CS+) was presented, followed in 33% of the cases by a painful electrodermal stimulation (unconditioned stimulus, US) to the back of the right hand (Fig. 1); alternatively, in the no-threat condition (NT), a square (unconditioned stimulus, CS−) was presented without any threat stimuli association. The two visual cues (CS+ and CS−) were presented in a pseudorandomized order for 5 seconds and were separated by a 5–10 second inter-stimulus interval (ITI) presentation of a black fixation cross on a white background.

The painful electrical stimuli (US) consisted of square wave pulses of 2 ms each, generated by a DS7A electrical stimulator (Digitimer) and were delivered through a surface electrode situated on the back of the right hand. Prior to the experiment, participant-specific painful stimulus intensity was determined by rating increasing stimulus intensities on a scale from 0 (no pain) to 10 (very painful). An intensity corresponding to pain 7 was used during the experiment.

At the end of every paradigm session the participants reported the amount of acquired fear, referring to their last encounter with each of the two visual cues (scaled to %, 0% = no anxiety, 100% = very anxious). These behavioral rating scales of fear were accompanied by the caption: "How much fear did you experience while looking at this figure?" There were no time constraints for providing ratings.

EEG recordings and TMS experiment. EEG signals were recorded continuously during experiments using a TMS-compatible direct current (DC)-coupling amplifier (Net Amps 300) and a high-density (256-channel) HydroCel Geodesic Sensor Net EEG recording system (EGI Netstation, Eugene, sampling rate: 250 Hz, impedances: ≤50 kOhms). To establish the intensity of the TMS stimulation (Magstim 200, Magstim Co., Whitland, Dyfed, UK), we first determined the resting motor threshold, defined as the minimum stimulus intensity at which the TMS pulse induced at least five motor evoked potentials (MEP) in ten consecutive trials[19]. MEPs were recorded on the left hand (contralateral hand to the TMS stimulation) abductor pollicis brevis muscle, using a tendon-belly arrangement. During the instructed fear paradigm, we applied the TMS pulses with intensity of 110% of the resting motor threshold[19].

The right dmPFC was targeted as defined in the individual MR images using a neuronavigation system (Localite, Sank Augustin) to the MNI coordinates ([10 12 58]) delimited in a previous fMRI activation study (Meyer *et al.*, unpublished). The MNI coordinates were registered and transformed to the subject-specific MRI using the SPM8 software (http://www.fil.ion.ucl.ac.uk/spm). After locating the stimulation site, the center of the TMS coil was placed tangentially to the scalp surface at the site of stimulation, with the coil oriented in a medial to lateral position at a 45° angle away from the midline with the handle pointing backwards. Based on previous findings[4,10,59], TMS was applied 1000 ms after each visual cue presentation (TMS experiment). At the end of the experiment we had a total of 90 trials, from which 36 belonged to the no-threat and 54 to the threat conditions, of which in 33% (18 trials) the painful stimuli was given and were not used in the subsequent analyses, leaving a total of 36 TMS pulses to be analysed for each condition. Further, as control for the TMS experiment, we applied the same instructed fear paradigm and recorded EEG signals without the addition of TMS. This experiment is referred as no-TMS experiment.

In order to ascertain the interpretability of the TMS-evoked responses to fear-responses, as well as to further test the feasibility of the measured evoked activity, a TMS experiment with an increased number of trials (N = 60) without any task involvement was conducted (see supplementary information).

EEG signal processing and analysis. To avoid contamination from TMS-related artefacts in the trials, EEG signals were processed as explained elsewhere (http://www.fieldtriptoolbox.org/tutorial/tms-eeg). First, 25 ms of TMS-related artefact (5 ms before and 20 ms after the TMS pulse) was removed from the EEG data.

Signals were then processed to account for line-noise and linear trends. Channels with high amplitudes over long time periods found during visual inspection were deleted trial-by-trial and scalp topology maps were used to further identify any remaining channels with artefacts to reject them, noisy channels were finally interpolated. All EEG analyses on the remaining channels were performed using a combination of FieldTrip (http://www.fieldtrip-toolbox.org/) and previously published in-house scripts[60]. Further detailed information on signal processing can be found in the extended methods section of the supplementary information. The artefact-free EEG data from both experiments was low-pass filtered with a cut-off frequency of 35 Hz and baseline corrected using the 500 ms prior to the visual cue. Event-related (ERP) and TMS-evoked potentials (TEPs) were then computed to identify peaks of activity at the corresponding time intervals of 0 to 1000 ms for ERPs and 1000 to 2000 ms for TEPs. The activity was considered a peak when at least 3 continuous points (12 ms) of the ERP waveform (on both sides) had smaller values. The amplitude at every peak was computed. Furthermore, the difference in amplitudes between threat (CS+ trials without the actual electric shock, US) and no-threat conditions (T-NT) was calculated and fed into further analyses as a marker of excitability-to-threat or dmPFC excitability regulation. To complement these measures, we computed the peak-to-peak differences, indicating the amplitude latency in between pairs of evoked components. For interpretational purposes we computed the TEPs using the same approach.

To ascertain the appropriate signal quality of the evoked potentials the SNR from a pool of all available trials for individual subject waveforms was computed as:

$$SNR_{EP} = 20 \ \log 10\left(\frac{\mathrm{TL}_{\mathrm{signal}}}{\mathrm{TL}_{\mathrm{noise}}}\right)$$

where $\mathrm{TL}_{\mathrm{signal}}$ is the mean activity within a time window of 500 ms containing the evoked waves, $\mathrm{TL}_{\mathrm{noise}}$ is the average signal at baseline, and SNR_{EP} is the SNR for the time window of interest expressed in decibels (dB), providing a straightforward measure that quantifies the signal strength of an evoked waveform[61]. A time window was used instead of the amplitude peaks since a single point estimate of SNR cannot fully portray the quality of an evoked activity, as it does not capture the variability of the signals[61]. Therefore, this calculation of SNR on signal averages is the most accurate representation of the evoked quality.

For our main study, the TMS experiment, we divided the scalp into frontal, dmPFC, occipital, central, parietal and temporal regions (Supplementary Fig. 1) and averaged data from the EEG channels from each of these regions.

Heart rate estimation. The heart rate estimation was done from the EEG signals using the extended version of the independent component analysis (ICA) algorithm[62] based on information maximization[63].

For EEG analysis, the rows of the input matrix y are the EEG signals recorded at the 256 electrodes, the rows of the output data matrix $v = X\,y$ are time courses of activation of the lCA components, and the columns of the inverse matrix, X^{-1}, give the projection strengths of the respective components onto the scalp sensors.

In general, and unlike principal component analysis (PCA), the component time courses of activation will be non-orthogonal. Corrected EEG signals can then be derived as $y' = (X)^{-1}v'$, where v' is the matrix of activation waveforms,v, with rows representing cardiac artefactual sources which are then extracted for further estimations from each participant. In total for the no-TMS experiment we concatenated the 36 CS+ trials without US to have 180 seconds and 24 CS- trials to have 120 seconds. The same was done for the TMS experiment.

MRI data analysis. The individual MRI data was pre-processed using the FreeSurfer software package v5.3 (https://surfer.nmr.mgh.harvard.edu/). The automated pipeline[64,65] included: (i) affine registration into Talairach space, (ii) intensity normalization for image inhomogeneities, (iii) removal of skull and non-brain tissues, (iv) definition of the gray/white matter and gray/cerebrospinal fluid boundaries, (v) surface creation and correction for topology defects and (vi) parcellation of the cortex and subcortical regions[66,67].

Data from all subjects was visually inspected for errors during pre-processing and manually corrected when necessary. Volumes of the dmPFC and insula, amygdala and hippocampus of both cerebral hemispheres were computed and corrected by head size in a fully-automated fashion. The anatomical delimitation of the dmPFC was performed according to Etkin, *et al.*[68], see Supplementary Fig. 2.

Statistical analyses. The fear ratings and registered heart rates were compared for differences between the threat and no-threat conditions using paired t-tests. The statistical significance of the differences between the amplitude of the TMS-evoked responses, fear ratings and heart rate for threat and no-threat conditions were corrected for multiple comparisons using FDR, whereas the spatial distribution of every evoked response across scalp locations was evaluated using non-parametric cluster-based statistics[69] with 1000 randomizations and a p-threshold of 0.05 to indicate channels within a cluster. After identification of significant amplitude differences, the dmPFC excitability-to-threat (see above) was extracted and further analyzed. Comparison of the cortical excitability-to-threat and dmPFC modulation in between the no-TMS and TMS data was carried out using t-test analyses. The effect sizes (d'), evaluated with the Cohen's d, are reported for all comparisons.

Furthermore, we adjusted multiple linear regression models to assess the predictive value of registered heart rates and the stress ratings to dmPFC excitability. The same models were used to investigate the anatomical substrates of the cortical excitability-to-threat and the dmPFC-related modulation. To avoid multicollinearity due to spurious correlations between different components of the evoked excitability-to-threat modulation, regression analyses were performed for each peak separately. Each excitability-to-threat peak was then regressed against the volume of the hippocampus, amygdala, insula and dmPFC. We applied a backward elimination in the regression

models, where predictors below a 10% significance level were deleted until none were left or statistical significance was reached. From these analyses the r^2 corresponding to the combined prediction is reported.

Only supra-threshold values obtained after correction for multiple comparisons (FDR $p < 0.05$) for condition testing and after contrasting the regression slopes against the null hypothesis (F-test, $p < 0.05$) for the regression analyses were considered as significant and reported in the manuscript.

Data Availability

The datasets generated during and/or analysed during the current study are available from the corresponding author on reasonable request.

References

1. Grillon, C. Models and mechanisms of anxiety: evidence from startle studies. *Psychopharmacology (Berl)* **199**, 421–437, https://doi.org/10.1007/s00213-007-1019-1 (2008).
2. Mechias, M. L., Etkin, A. & Kalisch, R. A meta-analysis of instructed fear studies: implications for conscious appraisal of threat. *NeuroImage* **49**, 1760–1768, https://doi.org/10.1016/j.neuroimage.2009.09.040 (2010).
3. Davis, M., Walker, D. L., Miles, L. & Grillon, C. Phasic vs sustained fear in rats and humans: role of the extended amygdala in fear vs anxiety. *Neuropsychopharmacology: official publication of the American College of Neuropsychopharmacology* **35**, 105–135, https://doi.org/10.1038/npp.2009.109 (2010).
4. Gable, P. A., Adams, D. L. & Proudfit, G. H. Transient tasks and enduring emotions: the impacts of affective content, task relevance, and picture duration on the sustained late positive potential. *Cognitive, affective & behavioral neuroscience* **15**, 45–54, https://doi.org/10.3758/s13415-014-0313-8 (2015).
5. Forscher, E. C., Zheng, Y., Ke, Z., Folstein, J. & Li, W. Decomposing fear perception: A combination of psychophysics and neurometric modeling of fear perception. *Neuropsychologia* **91**, 254–261, https://doi.org/10.1016/j.neuropsychologia.2016.08.018 (2016).
6. Herry, C. & Johansen, J. P. Encoding of fear learning and memory in distributed neuronal circuits. *Nat. Neurosci.* **17**, 1644–1654, https://doi.org/10.1038/nn.3869 (2014).
7. Hajcak, G., MacNamara, A. & Olvet, D. M. Event-related potentials, emotion, and emotion regulation: an integrative review. *Dev. Neuropsychol.* **35**, 129–155, https://doi.org/10.1080/87565640903526504 (2010).
8. Liu, Y., Huang, H., McGinnis-Deweese, M., Keil, A. & Ding, M. Neural substrate of the late positive potential in emotional processing. *J. Neurosci.* **32**, 14563–14572, https://doi.org/10.1523/JNEUROSCI.3109-12.2012 (2012).
9. Olofsson, J. K. & Polich, J. Affective visual event-related potentials: arousal, repetition, and time-on-task. *Biological psychology* **75**, 101–108, https://doi.org/10.1016/j.biopsycho.2006.12.006 (2007).
10. Gable, P. A. & Adams, D. L. Nonaffective motivation modulates the sustained LPP (1,000–2,000 ms). *Psychophysiology* **50**, 1251–1254, https://doi.org/10.1111/psyp.12135 (2013).
11. Hajcak, G. & Olvet, D. M. The persistence of attention to emotion: brain potentials during and after picture presentation. *Emotion* **8**, 250–255, https://doi.org/10.1037/1528-3542.8.2.250 (2008).
12. Pastor, M. C. *et al.* Affective picture perception: emotion, context, and the late positive potential. *Brain Res.* **1189**, 145–151, https://doi.org/10.1016/j.brainres.2007.10.072 (2008).
13. Etkin, A. & Wager, T. D. Functional neuroimaging of anxiety: a meta-analysis of emotional processing in PTSD, social anxiety disorder, and specific phobia. *Am. J. Psychiatry* **164**, 1476–1488, https://doi.org/10.1176/appi.ajp.2007.07030504 (2007).
14. Kamphausen, S. *et al.* Medial prefrontal dysfunction and prolonged amygdala response during instructed fear processing in borderline personality disorder. *The world journal of biological psychiatry: the official journal of the World Federation of Societies of Biological Psychiatry* **14**, 307–318, S301-304, https://doi.org/10.3109/15622975.2012.665174 (2013).
15. Kim, M. J. & Whalen, P. J. The structural integrity of an amygdala-prefrontal pathway predicts trait anxiety. *J. Neurosci.* **29**, 11614–11618, https://doi.org/10.1523/JNEUROSCI.2335-09.2009 (2009).
16. Maier, S. *et al.* Clarifying the role of the rostral dmPFC/dACC in fear/anxiety: learning, appraisal or expression? *PloS one* **7**, e50120, https://doi.org/10.1371/journal.pone.0050120 (2012).
17. Vytal, K. E., Overstreet, C., Charney, D. R., Robinson, O. J. & Grillon, C. Sustained anxiety increases amygdala-dorsomedial prefrontal coupling: a mechanism for maintaining an anxious state in healthy adults. *Journal of psychiatry & neuroscience: JPN* **39**, 321–329 (2014).
18. Groppa, S. *et al.* Subcortical substrates of TMS induced modulation of the cortico-cortical connectivity. *Brain stimulation* **6**, 138–146, https://doi.org/10.1016/j.brs.2012.03.014 (2013).
19. Groppa, S. *et al.* A practical guide to diagnostic transcranial magnetic stimulation: report of an IFCN committee. *Clinical neurophysiology: official journal of the International Federation of Clinical Neurophysiology* **123**, 858–882, https://doi.org/10.1016/j.clinph.2012.01.010 (2012).
20. Groppa, S. *et al.* The human dorsal premotor cortex facilitates the excitability of ipsilateral primary motor cortex via a short latency cortico-cortical route. *Hum. Brain Mapp.* **33**, 419–430, https://doi.org/10.1002/hbm.21221 (2012).
21. Rogasch, N. C. *et al.* Removing artefacts from TMS-EEG recordings using independent component analysis: importance for assessing prefrontal and motor cortex network properties. *NeuroImage* **101**, 425–439, https://doi.org/10.1016/j.neuroimage.2014.07.037 (2014).
22. Casula, E. P. *et al.* TMS-evoked long-lasting artefacts: A new adaptive algorithm for EEG signal correction. *Clinical neurophysiology: official journal of the International Federation of Clinical Neurophysiology* **128**, 1563–1574, https://doi.org/10.1016/j.clinph.2017.06.003 (2017).
23. Casula, E. P. *et al.* Transcranial direct current stimulation (tDCS) of the anterior prefrontal cortex (aPFC) modulates reinforcement learning and decision-making under uncertainty: a double-blind crossover study. *Journal of Cognitive Enhancement* **1**, 318–326 (2017).
24. Cattaneo, Z., Mattavelli, G., Platania, E. & Papagno, C. The role of the prefrontal cortex in controlling gender-stereotypical associations: a TMS investigation. *NeuroImage* **56**, 1839–1846, https://doi.org/10.1016/j.neuroimage.2011.02.037 (2011).
25. Notzon, S., Steinberg, C., Zwanzger, P. & Junghofer, M. Modulating Emotion Perception: Opposing Effects of Inhibitory and Excitatory Prefrontal Cortex Stimulation. *Biological psychiatry. Cognitive neuroscience and neuroimaging* **3**, 329–336, https://doi.org/10.1016/j.bpsc.2017.12.007 (2018).
26. Hill, A. T., Rogasch, N. C., Fitzgerald, P. B. & Hoy, K. E. TMS-EEG: A window into the neurophysiological effects of transcranial electrical stimulation in non-motor brain regions. *Neurosci. Biobehav. Rev.* **64**, 175–184 (2016).
27. Mattavelli, G., Rosanova, M., Casali, A. G., Papagno, C. & Romero Lauro, L. J. Top-down interference and cortical responsiveness in face processing: a TMS-EEG study. *NeuroImage* **76**, 24–32, https://doi.org/10.1016/j.neuroimage.2013.03.020 (2013).
28. Chang, W. H. *et al.* Optimal number of pulses as outcome measures of neuronavigated transcranial magnetic stimulation. *Clinical Neurophysiology* **127**, 2892–2897 (2016).

29. Goldsworthy, M., Hordacre, B. & Ridding, M. Minimum number of trials required for within-and between-session reliability of TMS measures of corticospinal excitability. *Neuroscience* **320**, 205–209 (2016).
30. Olofsson, J. K., Nordin, S., Sequeira, H. & Polich, J. Affective picture processing: an integrative review of ERP findings. *Biol. Psychol.* **77**, 247–265, https://doi.org/10.1016/j.biopsycho.2007.11.006 (2008).
31. Weinberg, A. & Hajcak, G. Beyond good and evil: the time-course of neural activity elicited by specific picture content. *Emotion* **10**, 767–782, https://doi.org/10.1037/a0020242 (2010).
32. Weinberg, A. & Hajcak, G. The late positive potential predicts subsequent interference with target processing. *J Cogn Neurosci* **23**, 2994–3007, https://doi.org/10.1162/jocn.2011.21630 (2011).
33. Cuthbert, B. N., Schupp, H. T., Bradley, M. M., Birbaumer, N. & Lang, P. J. Brain potentials in affective picture processing: covariation with autonomic arousal and affective report. *Biological psychology* **52**, 95–111 (2000).
34. Foti, D. & Hajcak, G. Deconstructing reappraisal: descriptions preceding arousing pictures modulate the subsequent neural response. *J Cogn Neurosci* **20**, 977–988, https://doi.org/10.1162/jocn.2008.20066 (2008).
35. Codispoti, M. & De Cesarei, A. Arousal and attention: Picture size and emotional reactions. *Psychophysiology* **44**, 680–686 (2007).
36. Azizian, A. & Polich, J. Evidence for attentional gradient in the serial position memory curve from event-related potentials. *J Cogn Neurosci* **19**, 2071–2081, https://doi.org/10.1162/jocn.2007.19.12.2071 (2007).
37. Dolcos, F. & Cabeza, R. Event-related potentials of emotional memory: encoding pleasant, unpleasant, and neutral pictures. *Cognitive, affective & behavioral neuroscience* **2**, 252–263 (2002).
38. Marini, F., Marzi, T. & Viggiano, M. P. "Wanted!" the effects of reward on face recognition: electrophysiological correlates. *Cognitive, affective & behavioral neuroscience* **11**, 627–643, https://doi.org/10.3758/s13415-011-0057-7 (2011).
39. Schupp, H. T., Flaisch, T., Stockburger, J. & Junghofer, M. Emotion and attention: event-related brain potential studies. *Prog. Brain Res.* **156**, 31–51, https://doi.org/10.1016/S0079-6123(06)56002-9 (2006).
40. Kalisch, R., Wiech, K., Critchley, H. D. & Dolan, R. J. Levels of appraisal: a medial prefrontal role in high-level appraisal of emotional material. *NeuroImage* **30**, 1458–1466, https://doi.org/10.1016/j.neuroimage.2005.11.011 (2006).
41. Bar-Haim, Y., Lamy, D. & Glickman, S. Attentional bias in anxiety: a behavioral and ERP study. *Brain and cognition* **59**, 11–22, https://doi.org/10.1016/j.bandc.2005.03.005 (2005).
42. Rogasch, N. C., Daskalakis, Z. J. & Fitzgerald, P. B. Cortical inhibition of distinct mechanisms in the dorsolateral prefrontal cortex is related to working memory performance: a TMS-EEG study. *Cortex* **64**, 68–77, https://doi.org/10.1016/j.cortex.2014.10.003 (2015).
43. Rogasch, N. C. & Fitzgerald, P. B. Assessing cortical network properties using TMS–EEG. *Hum. Brain Mapp.* **34**, 1652–1669 (2013).
44. Premoli, I. *et al*. TMS-EEG signatures of GABAergic neurotransmission in the human cortex. *J. Neurosci.* **34**, 5603–5612, https://doi.org/10.1523/JNEUROSCI.5089-13.2014 (2014).
45. Servan-Schreiber, D., Perlstein, W. M., Cohen, J. D. & Mintun, M. Selective pharmacological activation of limbic structures in human volunteers: a positron emission tomography study. *The Journal of neuropsychiatry and clinical neurosciences* **10**, 148–159, https://doi.org/10.1176/jnp.10.2.148 (1998).
46. LeDoux, J. E. Emotion circuits in the brain. *Annu. Rev. Neurosci.* **23**, 155–184, https://doi.org/10.1146/annurev.neuro.23.1.155 (2000).
47. Robinson, O. J., Charney, D. R., Overstreet, C., Vytal, K. & Grillon, C. The adaptive threat bias in anxiety: amygdala-dorsomedial prefrontal cortex coupling and aversive amplification. *NeuroImage* **60**, 523–529, https://doi.org/10.1016/j.neuroimage.2011.11.096 (2012).
48. Kalisch, R. *et al*. Context-dependent human extinction memory is mediated by a ventromedial prefrontal and hippocampal network. *J. Neurosci.* **26**, 9503–9511, https://doi.org/10.1523/JNEUROSCI.2021-06.2006 (2006).
49. Robinson, O. J. *et al*. The role of serotonin in the neurocircuitry of negative affective bias: serotonergic modulation of the dorsal medial prefrontal-amygdala 'aversive amplification' circuit. *NeuroImage* **78**, 217–223, https://doi.org/10.1016/j.neuroimage.2013.03.075 (2013).
50. Miniussi, C. & Thut, G. Combining TMS and EEG offers new prospects in cognitive neuroscience. *Brain topography* **22**, 249–256, https://doi.org/10.1007/s10548-009-0083-8 (2010).
51. Hallett, M. *et al*. Contribution of transcranial magnetic stimulation to assessment of brain connectivity and networks. *Clinical neurophysiology: official journal of the International Federation of Clinical Neurophysiology* **128**, 2125–2139, https://doi.org/10.1016/j.clinph.2017.08.007 (2017).
52. Komssi, S. & Kähkönen, S. The novelty value of the combined use of electroencephalography and transcranial magnetic stimulation for neuroscience research. *Brain Res. Rev.* **52**, 183–192 (2006).
53. Cavaleri, R., Schabrun, S. M. & Chipchase, L. S. The number of stimuli required to reliably assess corticomotor excitability and primary motor cortical representations using transcranial magnetic stimulation (TMS): a systematic review and meta-analysis. *Systematic reviews* **6**, 48 (2017).
54. Olsson, A. & Phelps, E. A. Learned fear of "unseen" faces after Pavlovian, observational, and instructed fear. *Psychol. Sci.* **15**, 822–828, https://doi.org/10.1111/j.0956-7976.2004.00762.x (2004).
55. Davey, C. G., Breakspear, M., Pujol, J. & Harrison, B. J. A Brain Model of Disturbed Self-Appraisal in Depression. *Am. J. Psychiatry* **174**, 895–903, https://doi.org/10.1176/appi.ajp.2017.16080883 (2017).
56. Scult, M. A., Knodt, A. R., Radtke, S. R., Brigidi, B. D. & Hariri, A. R. Prefrontal Executive Control Rescues Risk for Anxiety Associated with High Threat and Low Reward Brain Function. *Cereb. Cortex*, 1–7, https://doi.org/10.1093/cercor/bhx304 (2017).
57. Vialou, V. *et al*. Prefrontal cortical circuit for depression- and anxiety-related behaviors mediated by cholecystokinin: role of DeltaFosB. *J. Neurosci.* **34**, 3878–3887, https://doi.org/10.1523/JNEUROSCI.1787-13.2014 (2014).
58. Raczka, K. A. *et al*. Empirical support for an involvement of the mesostriatal dopamine system in human fear extinction. *Translational psychiatry* **1**, e12, https://doi.org/10.1038/tp.2011.10 (2011).
59. Meyer, B. *et al*. Neural mechanisms of placebo anxiolysis. *J. Neurosci.* **35**, 7365–7373, https://doi.org/10.1523/JNEUROSCI.4793-14.2015 (2015).
60. Chiosa, V. *et al*. Breakdown of Thalamo-Cortical Connectivity Precedes Spike Generation in Focal Epilepsies. *Brain connectivity* **7**, 309–320, https://doi.org/10.1089/brain.2017.0487 (2017).
61. Parks, N. A., Gannon, M. A., Long, S. M. & Young, M. E. Bootstrap Signal-to-Noise Confidence Intervals: An Objective Method for Subject Exclusion and Quality Control in ERPStudies. *Frontiers in human neuroscience* **10**, 50, https://doi.org/10.3389/fnhum.2016.00050 (2016).
62. Lee, T. Independent Component Analysis for Sub-Gaussian and Super-Gaussian Mixtures. proc. 4th Joint Symp. *Neural computation* **7**, 132–139 (1995).
63. Bell, A. J. & Sejnowski, T. J. An information-maximization approach to blind separation and blind deconvolution. *Neural Comput* **7**, 1129–1159 (1995).
64. Dale, A. M., Fischl, B. & Sereno, M. I. Cortical surface-based analysis. I. Segmentation and surface reconstruction. *NeuroImage* **9**, 179–194, https://doi.org/10.1006/nimg.1998.0395 (1999).
65. Fischl, B., Sereno, M. I. & Dale, A. M. Cortical surface-based analysis. II: Inflation, flattening, and a surface-based coordinate system. *NeuroImage* **9**, 195–207, https://doi.org/10.1006/nimg.1998.0396 (1999).
66. Fischl, B. *et al*. Whole brain segmentation: automated labeling of neuroanatomical structures in the human brain. *Neuron* **33**, 341–355 (2002).

67. Fischl, B. *et al*. Automatically parcellating the human cerebral cortex. *Cereb. Cortex* **14**, 11–22 (2004).
68. Etkin, A., Egner, T. & Kalisch, R. Emotional processing in anterior cingulate and medial prefrontal cortex. *Trends in cognitive sciences* **15**, 85–93, https://doi.org/10.1016/j.tics.2010.11.004 (2011).
69. Maris, E. & Oostenveld, R. Nonparametric statistical testing of EEG- and MEG-data. *J. Neurosci. Methods* **164**, 177–190, https://doi.org/10.1016/j.jneumeth.2007.03.024 (2007).

Acknowledgements
The authors thank Cheryl Ernest for proofreading the manuscript. The authors gratefully acknowledge the computing time granted on the supercomputer Mogon at Johannes Gutenberg University Mainz (hpc.uni-mainz.de). This work was supported by a grant from the German Research Council (DFG; CRC-TR-1193).

Author Contributions
S.G., M.M., B.M. and R.K. designed the experiment. G.G.E., M.M. and S.G. designed data-analysis methods. S.v.G., V.C.C. and T.B. performed the experiments. G.G.-E. analyzed the data. G.G.E. wrote the article. M.M. and S.G. revised the manuscript critically for important intellectual content. All the authors reviewed and accepted the contents of the manuscript.

Additional Information
Supplementary information accompanies this paper at https://doi.org/10.1038/s41598-018-32781-9.

Competing Interests: The authors declare no competing interests.

Publisher's note: Springer Nature remains neutral with regard to jurisdictional claims in published maps and institutional affiliations.

Open Access This article is licensed under a Creative Commons Attribution 4.0 International License, which permits use, sharing, adaptation, distribution and reproduction in any medium or format, as long as you give appropriate credit to the original author(s) and the source, provide a link to the Creative Commons license, and indicate if changes were made. The images or other third party material in this article are included in the article's Creative Commons license, unless indicated otherwise in a credit line to the material. If material is not included in the article's Creative Commons license and your intended use is not permitted by statutory regulation or exceeds the permitted use, you will need to obtain permission directly from the copyright holder. To view a copy of this license, visit http://creativecommons.org/licenses/by/4.0/.

© The Author(s) 2018